Composite Structures 281 (2022) 114987

Contents lists available at ScienceDirect

Composite Structures

journal homepage: www.elsevier.com/locate/compstruct

Bond performance of tensile lap-spliced basalt-FRP reinforcement in high-strength concrete beams

Islam Eltantawi [a], Wael Alnahhal [a,*], Ahmed El Refai [b], Adel Younis [c], Nasser Alnuaimi [a], Ramazan Kahraman [d]

[a] Department of Civil and Architectural Engineering, Qatar University, Qatar
[b] Department of Civil and Water Engineering, Laval University, Quebec, Canada
[c] Department of Building Technology, Faculty of Technology, Linnaeus University, Växjö, Sweden
[d] Department of Chemical Engineering, Qatar University, Doha, Qatar

ARTICLE INFO

Keywords:
Lap-splice
Fiber reinforced polymer (FRP)
Basalt FRP bars
High-strength concrete
Reinforced concrete beams
Bond

ABSTRACT

This paper investigates the bond between high-strength concrete (HSC) and tensile lap-spliced basalt fiber-reinforced polymer (BFRP) bars. Ten large-scale BFRP-reinforced concrete beams (300 × 450 × 3900 mm) were fabricated and tested under four-point loading until failure. The parameters investigated included the BFRP bar diameter (10, 12, and 16 mm), the splice length (400–1200 mm range), and the bar surface texture (sand-coated (SC) and helically wrapped (HW)). Test results demonstrated that the flexural capacity of the beams reinforced with SC-BFRP bars was almost similar to that of beams reinforced with HW-BFRP bars. However, SC-BFRP bars showed a slightly higher bond with concrete compared to that of helically wrapped counterparts. The bond strength of spliced BFRP bars was inversely related to the splice length. Also, BFRP bars with larger diameter bars require longer splice lengths to reach their maximum capacity. Finally, the experimentally estimated critical splice lengths were compared to those calculated by existing models and code-based equations. Both ACI 440.1R-15 and CSA S806-12 provisions were conservative in predicting splice length for BFRP bars. However, the CSA-S6-14 design code was more accurate in estimating the splice length for BFRP with bigger diameters. Though, it was not conservative with smaller diameters.

1. Introduction

Corrosion of steel reinforcement is a critical condition that causes the deterioration of reinforced concrete (RC) structures. In the Arabian Peninsula, corrosion of steel bars is more pronounced due to the high temperatures, severe humidity, and coastal exposure [1]. Accordingly, researchers and construction practitioners were motivated to investigate fiber-reinforced polymers (FRPs) as a durable alternative to steel bars in RC structures [2,3]. Compared to conventional steel, FRP bars are non-corrosive and are more resistant to weather and chemical exposures while having acceptable mechanical performance. FRPs are currently produced on a large scale, and design codes are being developed to promote and regulate their use in structural concrete [4–7].

Nonetheless, the wide use of FRPs is still limited compared to conventional steel because of their distinct physical and mechanical properties, not to mention their initial higher cost. Furthermore, FRP bars show brittle failure, lower modulus, and lower bond to concrete than their steel counterparts [8]. Such limitations in the mechanical characteristics of FRP bars have been successfully overcome with adequate assumptions and design guides.

FRP bars are produced with different surface textures, such as sand-coated (SC), ribbed, indented, helical wrapped (HW), and have been thoroughly investigated in terms of bond characterization [9–15]. The existing literature suggests that the bond between FRP bars and concrete is dependent on various parameters, including the surface roughness of the bars that determine the bar–concrete interlock, the chemical adhesion, and the loading conditions. Other key factors are the bars swelling due to temperature and moisture absorption [16–19]. Due to intrinsic variations in mechanical characteristics and surface textures, the current standards for steel bars cannot be applied to FRP bars. Likewise, the tensile lap splice of reinforcement bars is an important parameter that helps account for the limited bar lengths, especially in long-span members or construction joints [20,21]. Previous studies have determined that the bond strength between the reinforcing bars and concrete

* Corresponding author.
E-mail address: wael.alnahhal@qu.edu.qa (W. Alnahhal).

https://doi.org/10.1016/j.compstruct.2021.114987
Received 22 June 2021; Accepted 9 November 2021
Available online 14 November 2021

depends on several parameters such as the loading state, the environmental condition, the concrete strength, the transverse reinforcement, the bars spacing, the concrete cover, the bar diameter, and the embedment length [22–28]. A significant amount of research was devoted to determining the bond behavior and the lap splice length of FRP reinforcement in concrete [11–14]. Most of these studies have focused on the bond performance of Glass-FRP (GFRP) bars, the most utilized bars in the FRP family [29]. For instance, the effects of the bar surface and the concrete strength on the FRP-concrete bond were highlighted by Baena et al. [30]. They reported that the impact of bar surface treatment on bond strength is less significant when utilizing normal strength concrete vs. high strength concrete. However, Davalos et al. [31] stated that the concrete strength had little-to-no effect on the bond strength of FRP bars. Zemour et al. [32] reported that the current design guidelines and codes (i. e., JSCE-97 [33], CSA S806-12 [34], and ACI 440.1R-15 [35]) provided a reasonable prediction for the required GFRP splice length in GFRP-RC beams.

On the other hand, a limited number of studies have investigated the bond performance of basalt FRP (BFRP) bars [15,36–38]. El-Refai et al. [11] reported that SC-BFRP bars had a lower bond strength than SC-GFRP bars by about 25%. Moreover, Xiong et al. suggested [39] an equation to calculate the development length of the BFRP bars embedded in recycled aggregate concrete. The values calculated using this equation were 37% to 65% lesser than the values obtained using ACI 440.1R-06 provisions [40].

Furthermore, several studies recommended that FRP bars be utilized with high-strength concrete (HSC) [41]. For instance, Kalpana and Subramanian [42] observed that using HSC improved the performance of the GFRP-RC beams in terms of stiffness and load-carrying capacity. capacity Yost and Gross [43] stated that using HSC resulted in more effective utilization of the FRP reinforcement. This suggests HSC may be necessary in order to fully utilize the FRP bars. In addition, as HSC has higher durability and longer service life than normal strength concrete [44,45], combining HSC with a durable material such as BFRP bars can lead to a more durable structure.

Furthermore, it was obvious that the existing literature has focused on the use of GFRP bars and lacks experimental evidence on the bond performance of spliced BFRP reinforcement bars in reinforced concrete members. To the best of the authors' knowledge, this study is the first to address the bond performance of tensile lap-spliced BFRP reinforcement in HSC beams. The current design guidelines and codes concerning FRP-reinforced concrete (i.e., ACI 440.1–15 [35], CSA-S806-12 [34], and CSA-S6-14 [46]) do not account for BFRP bars in their lap splice/development length formulations. Accordingly, the current study aims to address this gap through an experimental investigation of the bond performance of lap-spliced BFRP reinforcement in HSC beams. For this, ten large-scale BFRP-RC beams, varying in bar diameter, bar surface, and splice length, were prepared and tested under four-point loading. Additionally, the experimental critical splice lengths of the tested beams were compared to those predicted by the existing guidelines and code-based equations.

2. Experimental program

2.1. Test specimens

Ten large-scale BFRP-RC beams were fabricated, as shown in Table 1. The beams were divided into two groups according to the BFRP bar surface. Beams of group 1 were reinforced with SC-BFRP longitudinal bars, while those of group 2 were reinforced with HW-BFRP bars. The beam dimensions were 300 mm in width, 450 mm in depth, and 3900 mm in length, as illustrated in Fig. 1. All beams were designed to have a tension-controlled failure in order to assure that the FRP bars will fail in tension first before the concrete breaks in compression. This is mostly due to the fact that the primary goal of this research is to evaluate the tension lap splicing of BFRP bars. The tension reinforcement consisted of two longitudinal BFRP bars spliced within the constant-moment region with different splice lengths, as stated in Table 1. In this study, three tension reinforcement ratios were used (0.74, 0.45 and 0.33 ρ_{bf} where ρ_{bf} is the balanced reinforcement ratio), as specified in Table 1. The balanced reinforcement ratio, ρ_{bf} was calculated according to CSA S806-12 provisions [34]. Two 8-mm diameter steel bars were used as top reinforcement. The lengths of the constant moment zones and the shear spans were 1700 and 900 mm, respectively. Steel stirrups of 10 mm diameter were provided at 150 mm spacing throughout the beam. As shown in Table 1, each specimen was labeled in the "X-Y-Z" format, where 'X' stands for the bar surface (SC = sand-coated and HW = helically wrapped, 'Y' represents the bar diameter (D = 10, 12, or 16 mm), and 'Z' represents the splice length (SL = 400–1200 mm range).

Table 1
Test matrix.

Specimen ID	Bar surface	No. and size of BFRP main bars	Reinforcement ratio, ρ_f	Splice length (mm)	Effective depth, d (mm)
Group 1					
SC-D10-SL400	Sand-coated	2–10 M	0.33 ρ_{fb}	400	395
SC-D10-SL600				600	
SC-D10-SL850				850	
SC-D12-SL500	Sand-coated	2–12 M	0.45 ρ_{fb}	500	394
SC-D12-SL700				700	
SC-D16-SL600	Sand-coated	2–16 M	0.74 ρ_{fb}	600	392
SC-D16-SL900				900	
SC-D16-SL1200				1200	
Group 2					
HW-D10-SL400	Helically wrapped	2–10 M	0.33 ρ_{fb}	400	395
HW-D10-SL600				600	

ρ_{bf} is the balanced reinforcement ratio.

2.2. Test setup and instrumentation

Fig. 2 shows the test setup of the beams. The beams were tested under four-point loading until failure. The load, deflection, and strain measurements were collected by an automatic acquisition system. Strain gauges of 5 mm length were placed on the longitudinal BFRP bars in the constant-moment zone. The strain gauges were installed along the splice at different locations, as shown in Fig. 3. The top surface of the concrete was also instrumented with 60-mm strain gauges to measure the compressive strains in concrete. The concrete strain gauges were placed at three locations along the lap splice zone at the constant-moment region, as shown in Fig. 3. Mid-span deflection was measured using linear variable differential transformers (LVDTs) that were placed on both sides of the beam. The loading rate was 1.2 mm/min and was conducted under displacement control.

2.3. Material properties

Ready-mix high-strength concrete was used to cast the beam specimens. The target compressive strength of concrete at 28-day age was 85 MPa. The design mix proportions were 437 kg/m^3 of ordinary Portland cement (OPC) with a water-to-cement ratio (w/c) of 0.3, 840 kg/m^3 of 20 mm Gabbro aggregates, 360 kg/m^3 of 10 mm Gabbro aggregates, and

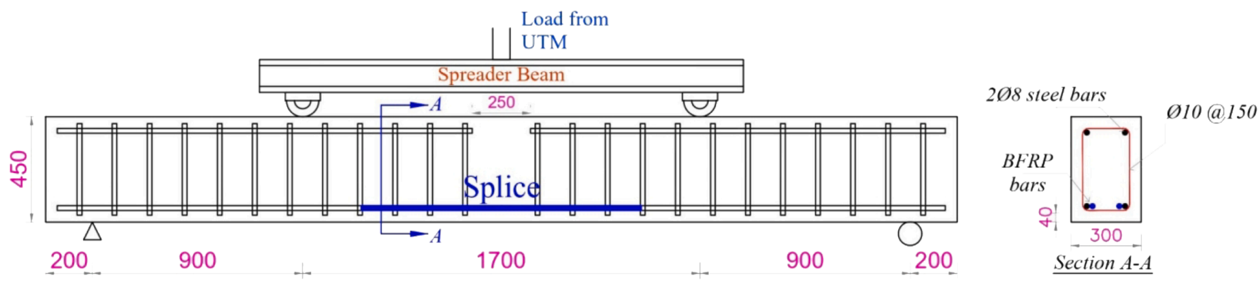

Fig. 1. Details of the tested beams (dimensions are in mm).

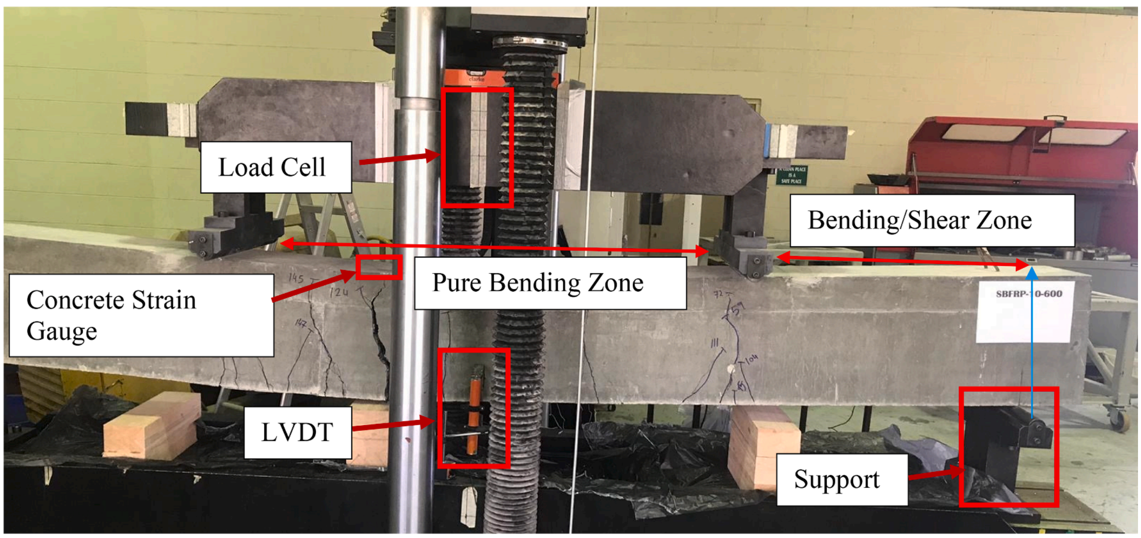

Fig. 2. Test setup for BFRP-RC beams.

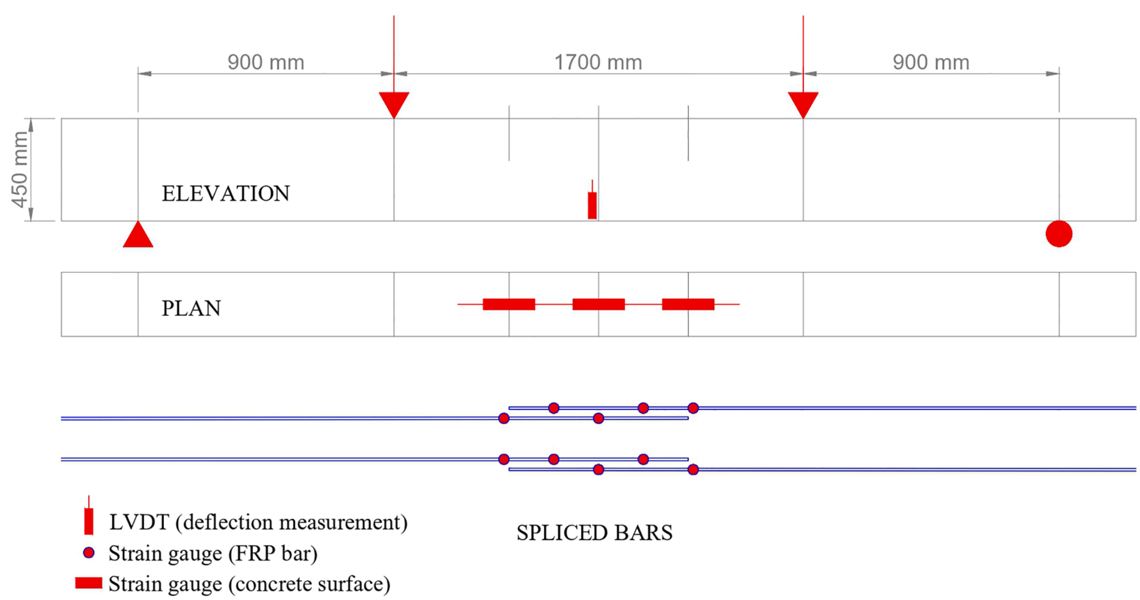

Fig. 3. Instrumentation details.

700 kg/m^3 sand. Three concrete cylinders (100 × 200 mm) and three concrete prisms (100 × 100 × 500 mm) were tested to determine the mechanical characteristics of hardened concrete. Compressive and flexural tensile strength tests were performed in accordance with ASTM C39 [47] and ASTM C78 [48], respectively. The test results revealed a 28-day compressive strength of 84.6 ± 0.62 MPa and flexural tensile strength of 7.38 ± 0.26 MPa.

Fig. 4 showed the texture of the BFRP bars used. Three bar diameters (10, 12, and 16 mm) were used for the SC texture and one bar diameter of 10 mm for the HW-BFRP bars. Twenty BFRP bar samples (i.e., five

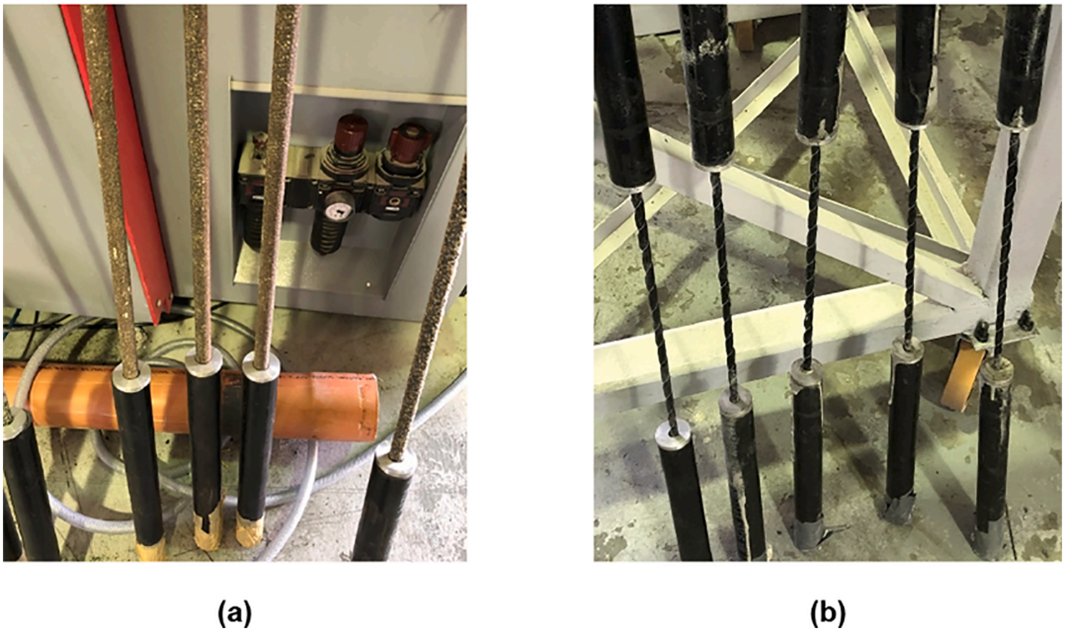

Fig. 4. (a) Sand-coated and (b) Helically-wrapped BFRP bars.

identical samples for each type) were tested in tension according to ASTM D7205 [49]. Fig. 5 (a) and (b) shows a SC-BFRP bar before and after testing, respectively. Table 2 presents the tensile properties of the BFRP bars used in the study.

Table 2
Properties of BFRP bars.

Bar	D10-SC	D12-SC	D16-SC	D10-HW
Surface	Sand-coated	Sand-coated	Sand-coated	Helically wrapped
Nominal diameter (mm)	10	12	16	10
Nominal area (mm^2)	78.54	113.1	201.06	78.54
Ultimate tensile strength (MPa)	1202.34 ± 59.44	1177.55 ± 164.4	1110.67 ± 83.74	1100 ± 19.41
Elastic modulus (GPa)	47.25 ± 0.2	49.48 ± 0.24	46.51 ± 0.27	44.41 ± 1.12
Ultimate strain (%)	2.54 ± 0.08	2.55 ± 0.13	2.38 ± 0.34	1.64 ± 0.19

3. RC beam test results

The BFRP-RC beams were tested in flexure while inspecting the critical splice length and the bond behavior. The outcomes of the experimental testing were expressed in terms of mid-span deflections, strains in both BFRP bars and concrete, the load-carrying capacity, the failure mode, the prediction of critical splice length, and its corresponding bond strength.

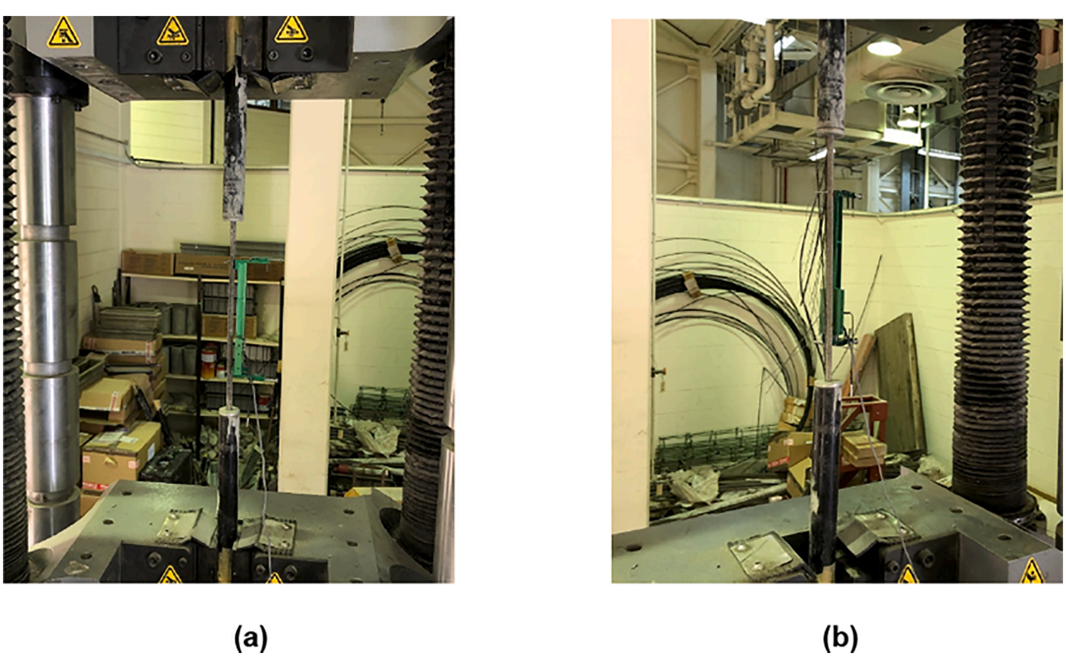

Fig. 5. (a) Sand-coated FRP bar before testing and (b) Sand-coated FRP bar after testing.

3.1. Load-deflection response

Fig. 6 (a) and (b) shows the load–deflection response of the tested BFRP-RC beams. It can be noticed that all beams showed a steep linear elastic behavior up to the formation of the first crack regardless of the surface texture, the splice length, or the bar diameter. The cracks formation increased in the constant moment region with the increment of the applied load, which was accompanied by a considerable degradation in the beams' stiffness. As expected, beams with longer splice lengths and higher reinforcement ratios showed less degradation in their stiffness. For instance, Specimen SC-D16-SL600 showed a deflection of 32 mm, while Specimen SC-D16-SL1200 had a deflection of 24.3 mm at an applied load of 160 kN, as shown in Fig. 6 (b). Likewise, the deflection of the beam SC-D10-SL600 reinforced with 10 mm bars was 34.4 mm, while the deflection of the SC-D16-SL600 reinforced with 16 mm bars was 13.1 mm at an applied load of 120 kN.

3.2. Load-carrying capacity

Table 3 lists the flexural capacities recorded for all of the tested specimens. As expected, the longitudinal reinforcement ratio showed a significant effect on the beam's flexural capacity. For instance, it can be

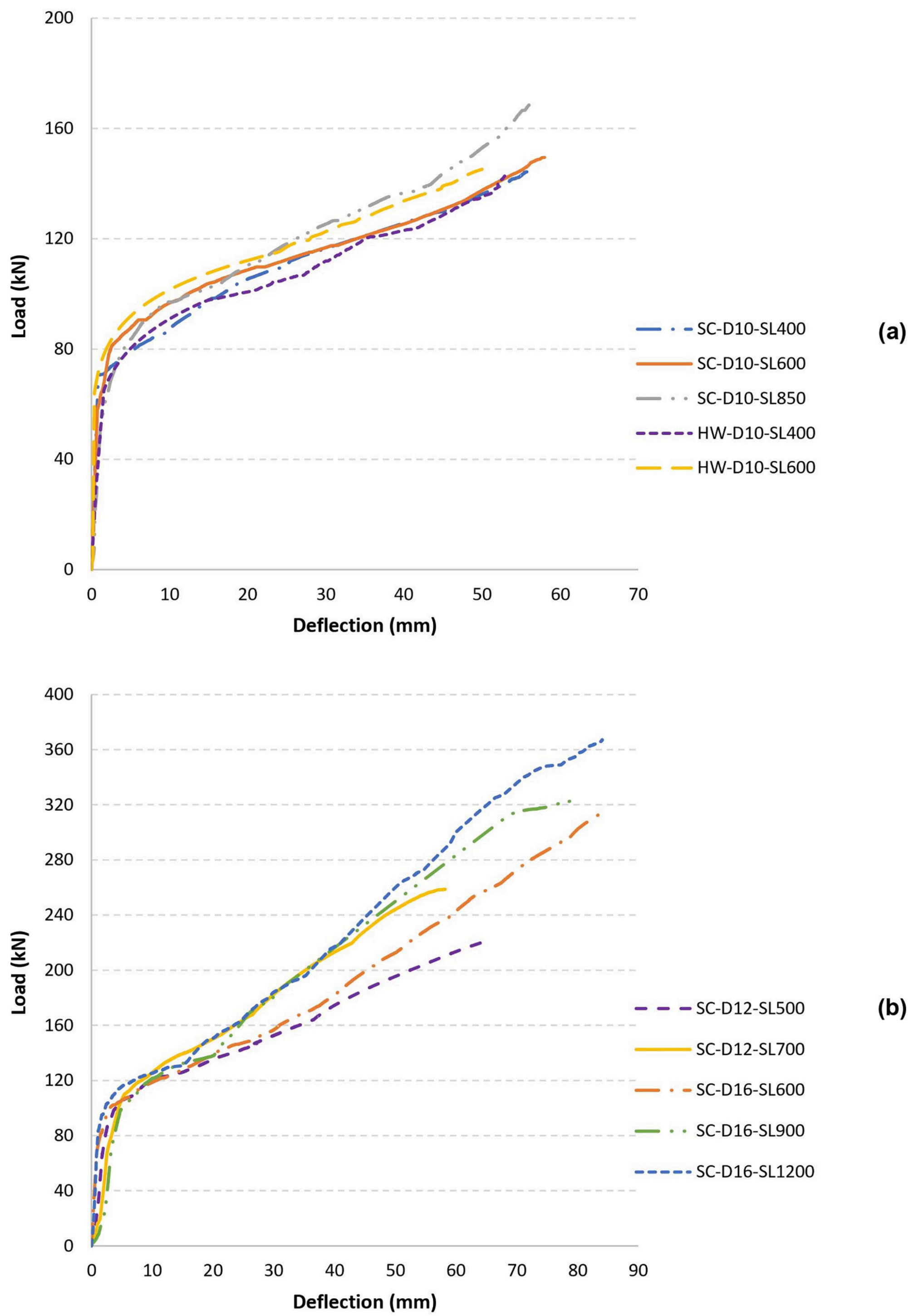

Fig. 6. Load-deflection responses of a) beams with 10 mm BFRP bars, and b) beams with 12 and 16 mm BFRP bars.

Table 3
Bond strengths, modes of failure, and experimental to predicted flexural capacities ratios for the tested beams.

Beam Identification	$M_{u,\exp.}$(kN.m)	CSA-S806-12 [34]		ACI-440.1–15 [35]		Mean bond strength (MPa)	Mean bond stress*(MPa)	Mode of failure
		$M_{u,pred.}$(kN.m)	$\frac{M_{u,pred.}}{M_{u,exp.}}$	$M_{u,pred.}$(kN.m)	$\frac{M_{u,pred.}}{M_{u,exp.}}$			
SC-D10-SL400	65.1	55	1.18	40	1.63	6.7	–	Debonding
SC-D10-SL600	67.3	55	1.22	40	1.68	4.6	–	Debonding
SC-D10-SL850	76.8	55	1.40	40	1.92	–	3.7	Rupture
SC-D12-SL500	99.28	78	1.27	56	1.77	6.8	–	Debonding
SC-D12-SL700	116.34	78	1.49	56	2.10	5.7	–	Debonding
SC-D16-SL600	142.19	126	1.13	93	1.53	6.2	–	Debonding
SC-D16-SL900	146.06	126	1.16	93	1.57	4.2	–	Debonding
SC-D16-SL1200	165.24	126	1.31	93	1.78	–	3.6	Rupture
HW-D10-SL400	65.25	50	1.31	36	1.82	6.6	–	Debonding
HW-D10-SL600	65.5	50	1.31	36	1.82	–	4.4	Rupture
Mean			1.28		1.76			
SD			0.11		0.16			
COV%			11.38		8.50			

* (at time of rupture)
$M_{u,\exp.}$ = Experimental ultimate moment; $M_{u,pred.}$ = Predicted ultimate moment

observed that specimen SC-D10-SL600 failed at a maximum load of 149.5 kN, while Specimen SC-D16-SL600 failed at a load higher than double that of the former (316 kN). In addition, the effect of the splice length can be demonstrated by comparing beams SC-D10-SL400, SC-D10-SL600, and SC-D10-SL850 in Group 1. The three beams had load-carrying capacities of 144.7, 149.5 and 170.6 kN, respectively. This indicates that having a longer splice length results in a relatively higher flexural strength.

On the other hand, it can be observed that the surface texture of BFRP bars had little-to-no effect on the flexural strength of the tested BFRP-RC beams. As an example, specimen SC-D10-SL400 with SC-BFRP bars had a load-carrying capacity of 144.7 kN, while specimen HW-D10-SL400 with HW-BFRP bars had a 145.19 kN capacity.

3.3. Modes of failure

Two distinct modes of failure were observed: BFRP/concrete debonding and BFRP rupture. The concrete/FRP debonding failure occurred in beams with a provided splice length less than the critical splice length, while the FRP rupture occurred mainly in the beams where an adequate splice length was provided. A typical debonding failure is shown in Fig. 7 (a). The debonding failure was associated with transverse and longitudinal cracks at the tension zone, as can be seen in Fig. 7 (a), and this failure was followed by pulling the bar out. On the other hand, Fig. 7 (b) depicts the visual observation of the FRP rupture.

3.4. Load-strain responses

Fig. 8 shows the measured strains of BFRP bars at different locations along the splice length for beam SC-D16-SL900. It also depicts the concrete strains at the top surface versus the applied load. It was noticed that the tensile strain measured at the end was greater than the strain recorded in the splice center as the BFRP bar attempts to slip from the ends. These findings suggest that bond stresses are focused at the end of the spliced FRP bars. On the other hand, Fig. 9 shows a comparison of the load–strain responses of all tested beams. The BFRP bar tensile strain was recorded at the splice end, while the concrete strain was recorded at the top surface at mid-span. In addition, Fig. 9 shows a variation in the strain readings depending on the status of the beam, whether it is over-spliced (having a splice length that is longer than the theoretically necessary length) or under-spliced (having a splice length that is less than the theoretically necessary length). It was noticed that the over-spliced beams exhibited higher strain than the under-spliced beams. Additionally, ultimate strains in BFRP bars increased with the increase in the splice length. Furthermore, test results showed that SC-BFRP bars exhibited higher ultimate tensile strains than that of HW-BFRP bars, particularly for beams with larger diameter bars [50–52].

3.5. Bond strength assessment

The bond between the spliced bars and the concrete governs the transfer of tensile force between them. When the concrete splits around the spliced bar, the bond between them fails. Fig. 10 shows how the bond strength of the spliced BFRP bars in concrete is affected by the bar diameter and the splice length. The bond strength between the FRP bar and concrete within the spliced area was calculated by dividing the bar's tensile force over the surface area of the bar within the spliced zone. Accordingly, the bond stress was calculated using the following equation, assuming that the distribution of the bond was uniform along the spliced length of the FRP bar [53,54]:

$$\mu = \frac{df_s}{4l_s} \tag{1}$$

where μ is the bond stress (MPa), d is the diameter of the FRP bar (mm),

$f_s$is the developed stress in the bar (MPa), and l_s is the splice length (mm).

$$f_s = \frac{M_a}{A_f jd} \tag{2}$$

$$jd = d - \frac{kd}{3} \tag{3}$$

$$k = \sqrt{(\rho_{frp}n_{frp})^2 + 2\rho_{frp}n_{frp}} - \rho_{frp}n_{frp} \tag{4}$$

where M_a is the applied moment (kN.m), A_f is the FRP reinforcement's area (mm^2), jd is the moment arm (mm), d is the distance from the concrete surface to the tension bar center (mm).

The bond stresses and splice length were shown to have an inverse relationship under a given load. The decrease in bond stresses with increasing splice length is attributable to the increase in frictional and mechanical interlock resistances along the embedment length. Similar behavior was reported by other researchers [9–13]. Furthermore, there is a direct relationship between the bond stress and the FRP bar diameters in a given beam geometry. The bond strength is calculated by dividing the maximum force (F_{max}) over the surface area of the bar

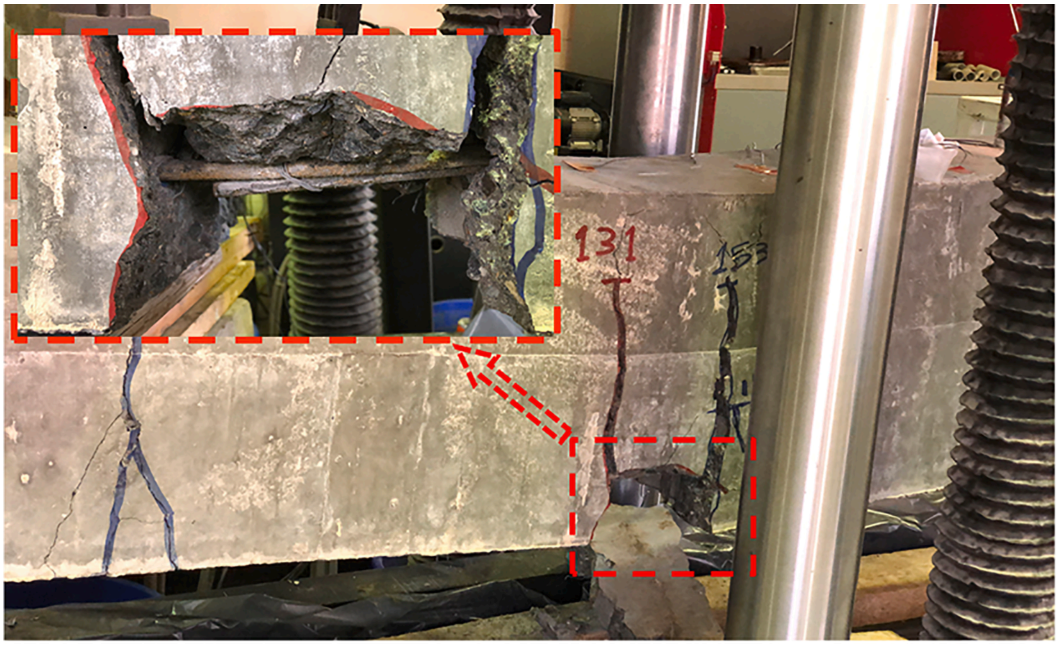

(a)

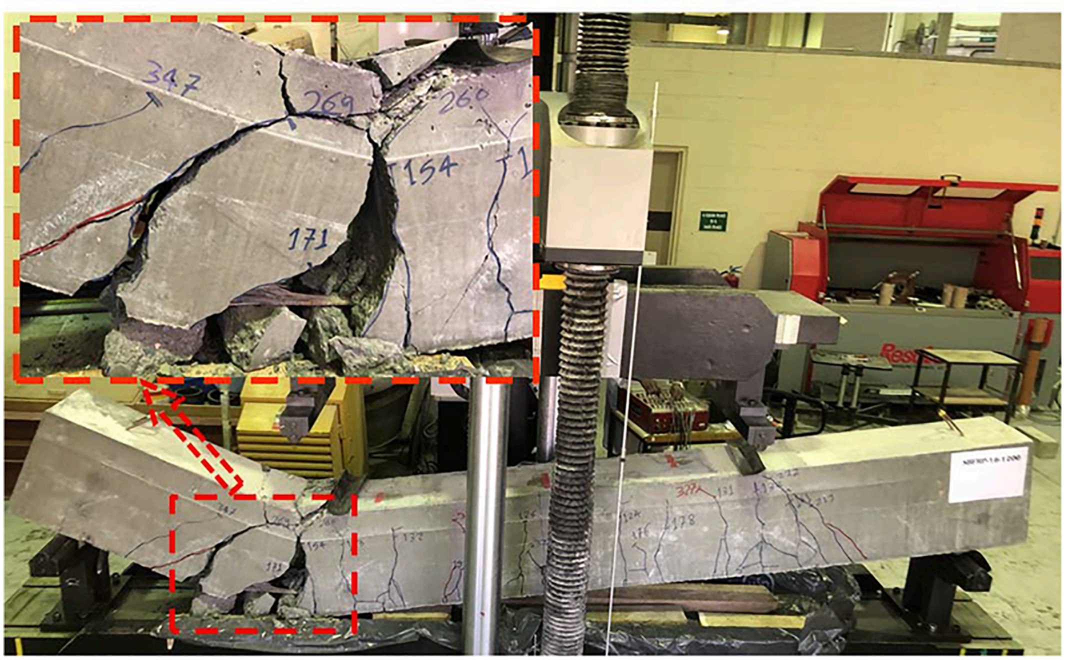

(b)

Fig. 7. Modes of failure: (a) Delamination/Debonding of concrete at the tension zone and (b) BFRP tensile rupture.

($\pi^*d^*l_s$). Thus, the larger the diameter, the higher the bar surface area and the maximum force. However, the increment in the maximum force is higher than the increment in the surface area, which yields in an overall escalation in the bond strength [39]. For example, the critical bond stresses (i. e., bond strengths) for the SC- BFRP bars of 10 and 16 mm diameters, with a splice length of 600 mm, are 4.6 and 6.2 MPa, respectively.

Comparing the sand-coated bars to the helically wrapped bars shows that the former had a slightly higher bond strength. This is because the surface roughness of the sand-coated improves the bond characteristics with the surrounding concrete. This observation was confirmed by Saleh et al. [14].

3.6. Experimental measurement of critical splice length

Fig. 11 depicts the applied force versus the strain for three beams reinforced with SC-BFRP bars with a diameter of 16 mm. The theoretical load versus strain response was drawn (solid line) by applying the ultimate strength analysis. It can be observed that the measured experimental strains were close to the theoretical values. Accordingly, the

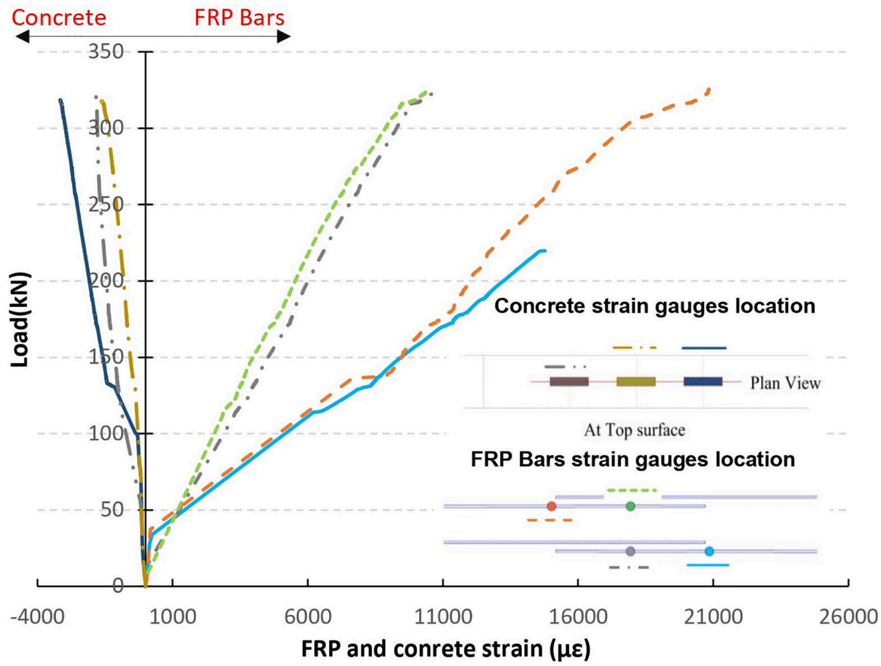

Fig. 8. Load-strain responses for beam SC-D16-SL900.

maximum strain in the spliced FRP bars can also be predicted by means of flexural strength analysis.

Fig. 12 (a), (b), and (c) show the maximum strains at the ends of the spliced BFRP bars versus splice length for the SC-BFRP bars with 10, 12, and 16 mm diameters, respectively. Fig. 12 (d) exhibits the maximum strains at the ends of the spliced BFRP bars versus splice length for the HW-BFRP bars with 10 mm diameter. The results defined a direct linear relationship between the maximum strains (at the ends of the spliced bars) and the splice length. By linearly fitting the points of the test results, a sloped line was drawn which intersects two lines: the first of which (dashed) represents the minimum allowable strain, and the second one (solid) represents the maximum allowable strain. The continuous vertical line in Fig. 12 (a), (b), (c), and (d) indicates the required splice length. This value is the critical splice length (l_s) obtained experimentally.

4. Predictions of flexural strength and critical splice length

4.1. Prediction of flexural strength

The beams were designed to have a tension-controlled failure. This was confirmed as the concrete strain in all tested beams was less than the ultimate concrete strain. Using ACI-440.1–15 provisions [35], the theoretical flexural capacities of the tested beams were calculated based on the following equation:

$$M_u = \phi M_n = A_f f_{Fu}\left(d - \frac{\beta_1 c_b}{2}\right) \tag{5}$$

$$c_b = \left(\frac{\varepsilon_{cu}}{\varepsilon_{cu} + \varepsilon_{Fu}}\right) d \tag{6}$$

where M_u is the ultimate moment (kN.m),$\phi = 0.65$, A_f is the FRP reinforcement's area (mm^2), f_{Fu} is the FRP bar's tensile strength in MPa, d is the distance from the concrete surface to the tension bar center, $\beta_1 = 0.675$ for $f'_c = 85$ MPa, ε_{cu} is the ultimate strain of concrete $= 0.003$, and ε_{Fu} is the ultimate strain of the FRP bar.

For the CSA S806-12 design guide, the theoretical values of the moment were calculated based on the following equation:

$$M_u = \phi_f A_f (\varepsilon_{Fu} E_{FRP})\left(d - \frac{\beta c}{2}\right) \tag{7}$$

The theoretical ultimate bending moment was estimated assuming a perfect bond between concrete and FRP reinforcement. Table 3 summarizes the results of the experimental and predicted flexural moment capacities of the tested beams.

By comparing the experimental to predicted capacities, it can be observed that both the CSA-S806-12 [34] and ACI-440.1–15 [35] underestimate the ultimate capacities of the beams which yields a more conservative design. Also, it can be noticed that the CSA-S806-12 [34] design guides provided a more accurate prediction of the flexural capacities of the beams compared to the ACI-440.1–15 [35] provisions, as shown in Table 3.

4.2. Prediction of critical splice length

The developmental length (l_d) is classically recognized in the existing design codes as an indication of the required lap splice. According to CSA S806-12 [34], the development length (l_d, in mm) of FRP bars is calculated as follows:

$$l_d = 1.15 \frac{k_1 k_2 k_3 k_4 k_5}{d_{cs}} \frac{f_F}{\sqrt{f'_c}} A_{Fb} \tag{8}$$

where A_{Fb} is the FRP reinforcement's area (mm^2), f_F is the FRP bar's tensile strength in MPa, f'_c is the concrete strength in MPa, k_1 is a factor for the bar location (taken as 1.3 for the horizontally placed reinforcement and 1.0 for other conditions), k_2 is a factor for the density of concrete (taken respectively as 1.3, 1.2, and 1.0 for low, semi-low, and normal densities), k_3 represents the effect of the bar size ($k_3 = 0.8$ for $A_{Fb} < 300$ mm^2 and 1.0 for A_{Fb} greater than 300 mm^2), k_4 represents the effect of the bar fiber ($k_4 = 1.0$ for carbon/glass-FRP and 1.25 for aramid-FRP), k_5 represents the bar surface profile ($k_5 = 1.0$ for the braided/roughened/sand-coated surfaces, 1.05 for the surfaces that are ribbed or have a spiral pattern, and 1.8 for the indented surfaces), and d_{cs} is the minimum distance from the nearest concrete surface to the bar center (not to exceed two-third of the center-to-center bar spacing). The

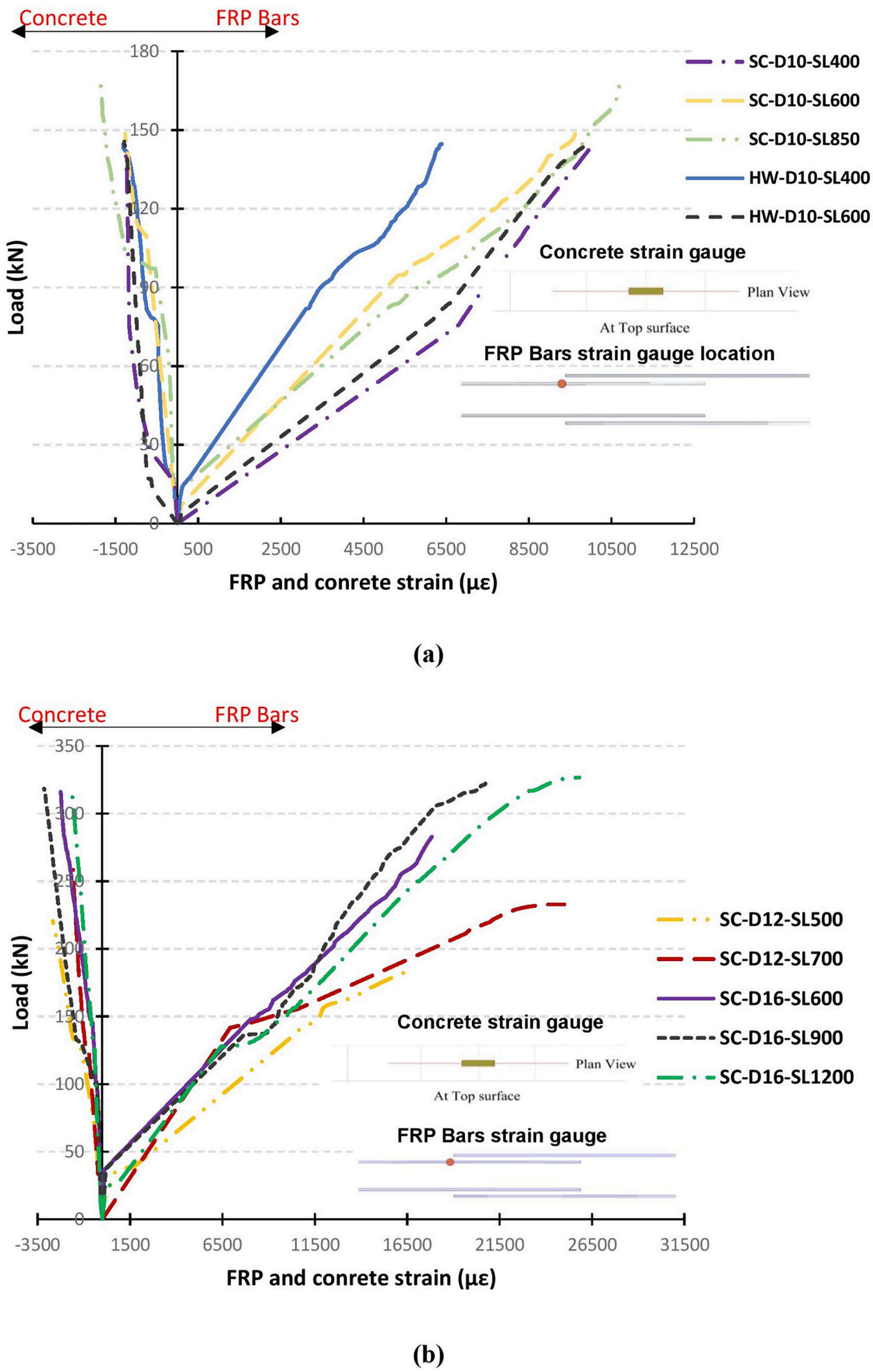

Fig. 9. Load-strain responses of a) beams with 10 mm BFRP bars, and b) beams with 12 and 16 mm BFRP bars.

factors d_{cs} and $\sqrt{f_c^{'}}$ shall not exceed $2.5d_b$ and 5 MPa, respectively.

The development length according to CSA S6-14 [46] is calculated as follows:

$$l_d = 0.45\frac{k_1 k_4}{\left[d_{cs} + K_{tr}\frac{E_F}{E_s}\right]}\left[\frac{f_{Fu}}{f_{cr}}\right]A_{Fb} \tag{9}$$

$$K_{tr} = 0.45\frac{A_{tr}f_y}{10.5sn} \tag{10}$$

where $f_{cr} = 0.4\sqrt{f_c^{'}}$ is concrete's cracking strength in MPa ($\leq$3.2 MPa), k_4 represents the effect of the bar surface, as it is a representation of the bond-strength ratio of FRP bars to that of deformed steel bars with the same cross-sectional area ($k_4 = 0.8$ in the absence of experimental data and k_4 does not exceed 1), A_{tr} is the area of stirrups in mm^2, f_y is the transverse reinforcement yield strength in MPa for steel stirrups and that will change to f_{Fu} for FRP transverse reinforcment. The term $\left[d_{cs} + K_{tr}\frac{E_F}{E_s}\right]$ shall not exceed $2.5d_b$.

The development length as per ACI 440.1R-15 [35] is given by:

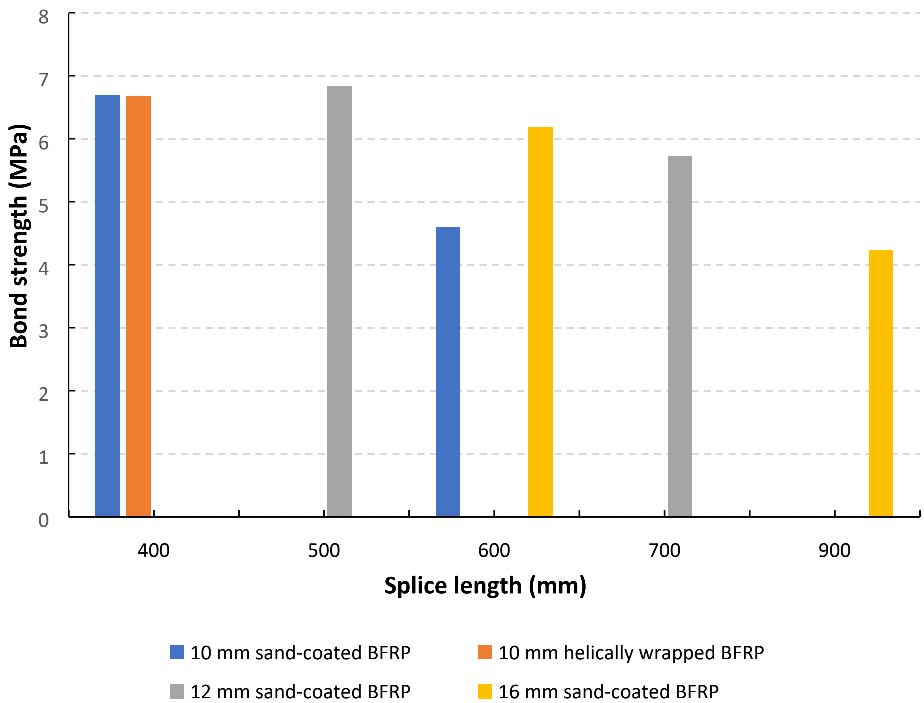

Fig. 10. Average bond stress at failure versus splice length of the tested beams.

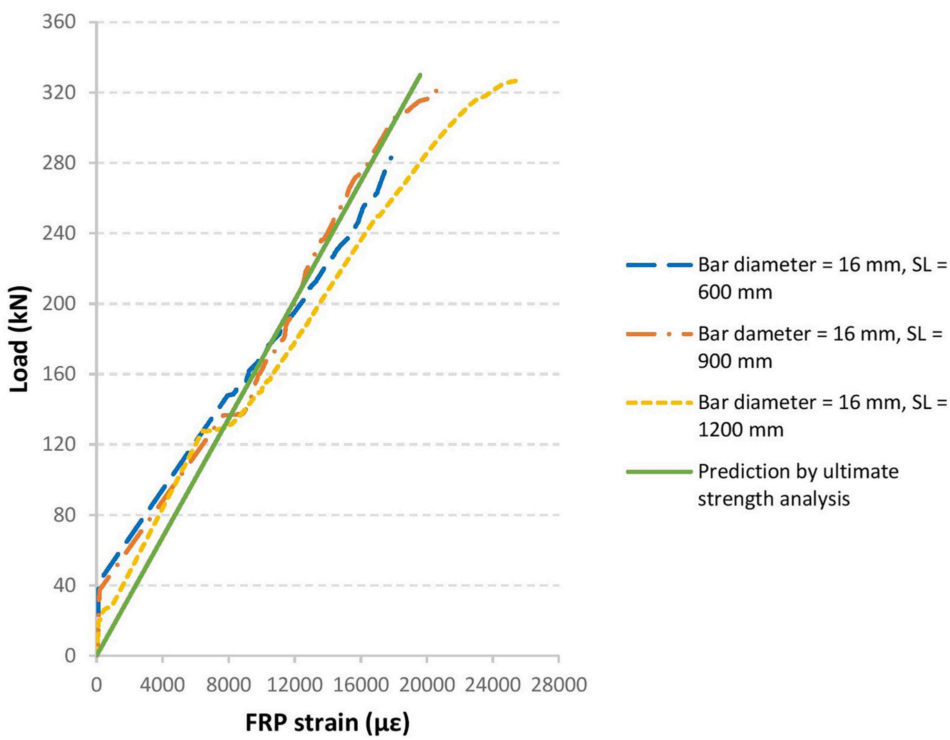

Fig. 11. Prediction of strain at the end of splice length.

$$l_d = \frac{\alpha \frac{f_{Fr}}{0.083\sqrt{f'_c}} - 340}{13.6 + \frac{C}{d_b}} d_b \tag{11}$$

Where $f_{Fr} = C_E f_{Fu}$ (C_E is an environmental reduction factor), α is the bar location factor ($\alpha = 1.5$ when more than 300 mm of fresh concrete is cast below the reinforcement bars, and 1.0 otherwise), and $C = \min\left(d_c, \frac{c/cspacing}{2}\right) \leq 3.5 d_b$.

The critical splice lengths (l_s) which equal to 1.3 times the development lengths (l_d), were calculated according to CSA S806-12 [34], CSA-S6-14 [46], and ACI 440.1R-15 [35] provisions, using the obtained development length from equations (8), (9), and (11), respectively. Three diameters were considered: 10, 12, and 16 mm for SC-BFRP bars and 10 mm for HW-BFRP bars. Table 4 summarizes the values of the critical splice lengths based on the design guidelines and code-based equations mentioned above. It was noticed that the estimated critical

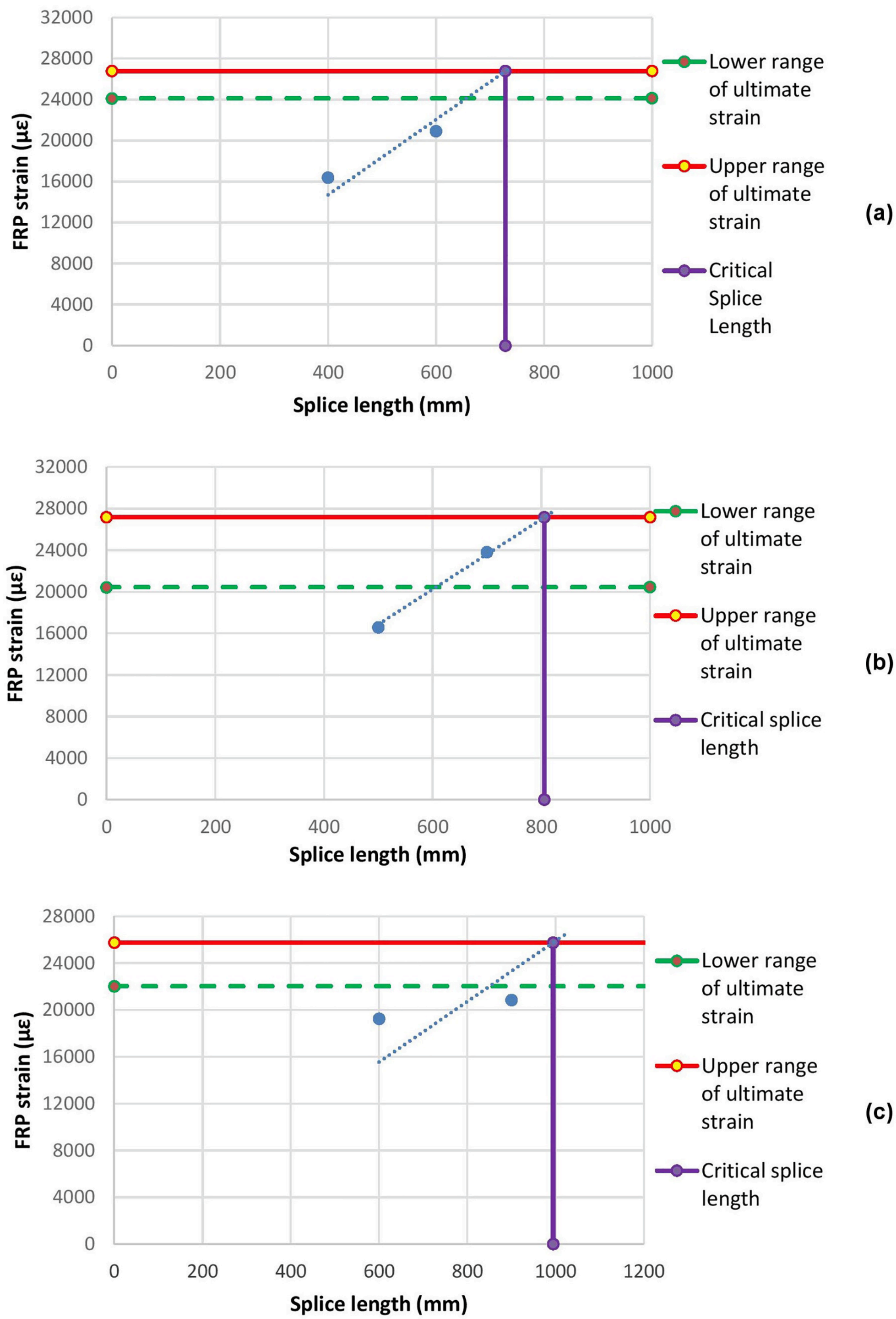

Fig. 12. Typical strain variation versus splice length of (a) 10 mm, (b) 12 mm, (c) 16 mm diameter SC-BFRP bars, and (d) 10 mm HW-BFRP bars.

splice lengths based on the CSA-S806-12 [34] and the ACI 440.1R-15 [35] were almost the same, while the estimated values using the CSA S6-14 [46] equation notably differ from them. It can be seen that the larger the diameter, the higher the required splice length. Also, the sand-coated bars require a longer splice length than the helically wrapped bars as the ultimate tensile strength of SC-BFRP bars is higher than that of HW-BFRP bars used in this study. It is worth mentioning that the above three design guidelines and codes do not take the BFRP bars or the helically wrapped texture into account.

Furthermore, Table 4 depicts a comparison between the predicted splice lengths using the aforementioned equations and the experimentally calculated splice lengths. It was noticed that the ACI 440.1R-15 [35] and CSA S806-12 [34] equations overestimated the critical splice lengths by nearly 25% for the SC-BFRP bars and almost 15% for the HW-BFRP bars. However, the CSA-S6-14 [46] equation, while using $k_4 = 0.8$, underestimated the critical splice length. The CSA-S6-14 [46] equation, on the other hand, offer more accurate estimates for the critical splice length when $k_4 = 1.0$, with a slight underestimate for bars with 10 mm diameter. As a result, using ACI 440.1R-15 [35] and CSA S806-12 [34] formulae for all tested beams is conservative. In addition,

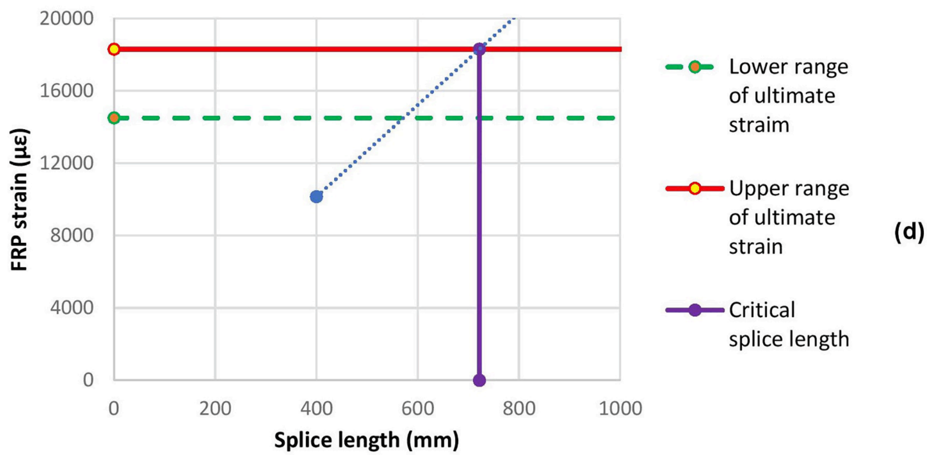

Fig. 12. (*continued*).

Table 4
Experimental and Predicted critical splice lengths of BFRP bars.

	Type of the bar	D10-SC	D12-SC	D16-SC	D10-HW
Experimental	Critical splice length, Experimental (l_s, exp.), (mm)	≃ 695	≃ 815	≃ 1025	≃ 720
CSA S806-12 [34]	Splice Length, predicted (l_s, pred.), (mm)	903.52 **≃ 905**	1061.87 **≃ 1100**	1335.41 **≃ 1340**	867.94 **≃ 870**
	$\frac{l_s,\text{exp.}}{l_s,\text{pred.}}$	0.77	0.74	0.76	0.83
CSA-S6-14 [46], k_4=0.8	Splice Length, predicted (l_s, pred.), (mm)	552.42 **≃ 555**	649.24 ≃ **650**	816.49 ≃ **820**	505.40 **≃ 510**
	$\frac{l_s,\text{exp.}}{l_s,\text{pred.}}$	1.25	1.25	1.25	1.41
CSA-S6-14 [46], k_4=1.0	Splice Length, predicted (l_s, pred.), (mm)	690.53 **≃ 695**	811.55 ≃ **815**	1020.61 **≃ 1025**	631.75 **≃ 635**
	$\frac{l_s,\text{exp.}}{l_s,\text{pred.}}$	1.05	0.99	0.97	1.13
ACI 440.1R-15 [35]	Splice Length, predicted (l_s, pred.), (mm)	936.02 **≃ 940**	1093.67 **≃ 1095**	1361.87 **≃ 1365**	834.35 **≃ 835**
	$\frac{l_s,\text{exp.}}{l_s,\text{pred.}}$	0.74	0.74	0.75	0.86

test results indicate that the BFRP bars can be treated similarly to the CFRP and the GFRP bars when using the CSA S806-12 [34] equations. It is important to note that the environmental reduction factor C_E was taken as 1 in the ACI440.1–15 equation [35] for the basalt as the tests were held in a controlled environment. However, future research is encouraged to investigate the BFRP/concrete bond under long-term exposures.

5. Conclusions

The bond behavior of tensile lap-spliced BFRP bars in high-strength concrete beams was experimentally investigated. Ten BFRP-RC beams were tested under 4-point loading until failure. The critical splice lengths of the tested beams were predicted using the equations of current design guidelines and codes. Based on the study results, the following conclusions have been drawn:

- The load-carrying capacity of the beams reinforced with SC-BFRP bars was nearly identical to that of the beams reinforced with HW-BFRP bars of the same splice length.
- The surface texture of BFRP bars had a slight impact on the BFRP/concrete bond and, as a result, the critical splice length. The measured bond strength of the SC-BFRP bars was slightly higher than that of the HW-BFRP bars. Therefore, the required splice length for HW-BFRP bars was around 5% above that of the SC-BFRP bars.
- The bond strength of spliced BFRP bars is inversely proportional to the splice length. For example, increasing the lap splice length from 400 mm to 600 mm reduced the bond strength by 33%.
- Larger diameter bars, as anticipated, require a longer splice length to reach their maximum capacity. These findings suggest that using bars with smaller diameters improves the bond capacity of the splice.
- The ultimate strength analysis can be utilized to estimate stresses at the ends of spliced BFRP bars in high-strength concrete.
- ACI 440.1R-15 [35] and CSA S806-12 [34] equations, assuming the fabric type factor = 1.0 (equivalent to glass/carbon fabric owing to a lack of experimental data for basalt fabric), are conservative in predicting splice length for BFRP bars. The CSA-S6-14 [46] equation, on the other hand, is more accurate in estimating the splice length for BFRP with bigger diameters. It is not, however, conservative with smaller diameters.

The authors would like to stress that the conclusions presented above are entirely based on the experimental results of the BFRP bars utilized in this investigation. Without experimental validation, the results of these tests should not be applied to beams reinforced with different types of BFRP bars than those employed in the testing. As a result, further experimental data is needed to confirm these findings utilizing other types of BFRP bars with varying diameters, surface textures, and splice lengths. Future research should focus on the long-term durability and bond performance of tensile lap-spliced BFRP bars utilized in this study under diverse environmental conditions.

Declaration of Competing Interest

The authors declare that they have no known competing financial interests or personal relationships that could have appeared to influence the work reported in this paper.

Acknowledgment

The authors show their gratitude to Qatar University for their financial support through the internal grant no. QUCG-CENG-20/21-3. The findings achieved herein are solely the responsibility of the authors. Open Access funding provided by the Qatar National Library.

Data Availability

Data availability The raw/processed data required to reproduce these findings cannot be shared at this time as the data also forms part of an ongoing study.

References

[1] Al-Samarai M. Durability of Concrete in the Arabian Gulf. J Mater Sci Eng A 2015; 5:11–2. https://doi.org/10.17265/2161-6213/2015.11-12.003.

[2] Attia K, Alnahhal W, Elrefai A, Rihan Y. Flexural behavior of basalt fiber-reinforced concrete slab strips reinforced with BFRP and GFRP bars. Compos Struct 2019;211: 1–12. https://doi.org/10.1016/j.compstruct.2018.12.016.

[3] Attia K, El Refai A, Alnahhal W. Flexural Behavior of Basalt Fiber-Reinforced Concrete Slab Strips with BFRP Bars: Experimental Testing and Numerical Simulation. J Compos Constr 2020;24(2):04020007. https://doi.org/10.1061/(ASCE)CC.1943-5614.0001002.

[4] Cosenza E, Manfredi G, Realfonzo R. Development length of FRP straight rebars. Compos Part B Eng 2002;33(7):493–504. https://doi.org/10.1016/S1359-8368(02)00051-3.

[5] Aref A, Alnahhal W. Experimental Evaluation of a Hybrid FRP-Concrete Bridge Superstructure System Under Negative Moment Flexural Loads. Jordan J Civ Eng 2007;1:336–43.

[6] Al-Hamrani A, Alnahhal W. Shear behavior of basalt FRC beams reinforced with basalt FRP bars and glass FRP stirrups: Experimental and analytical investigations. Eng Struct 2021;242:112612. https://doi.org/10.1016/j.engstruct.2021.112612.

[7] Abushanab A, Alnahhal W, Farraj M. Structural performance and moment redistribution of basalt FRC continuous beams reinforced with basalt FRP bars. Eng Struct 2021;240:112390. https://doi.org/10.1016/j.engstruct.2021.112390.

[8] Guedes RM, Xavier J. In: Advanced Fibre-Reinforced Polymer (FRP) Composites for Structural Applications. Elsevier; 2013. p. 298–360. https://doi.org/10.1533/9780857098641.3.298.

[9] Achillides Z, Pilakoutas K. Bond Behavior of Fiber Reinforced Polymer Bars under Direct Pullout Conditions. J Compos Constr 2004;8(2):173–81. https://doi.org/10.1061/(ASCE)1090-0268(2004)8:2(173).

[10] Hao Q, Wang Y, He Z, Ou J. Bond strength of glass fiber reinforced polymer ribbed rebars in normal strength concrete. Constr Build Mater 2009;23(2):865–71. https://doi.org/10.1016/j.conbuildmat.2008.04.011.

[11] El Refai A, Ammar M-A, Masmoudi R. Bond Performance of Basalt Fiber-Reinforced Polymer Bars to Concrete. J Compos Constr 2015;19(3):04014050. https://doi.org/10.1061/(ASCE)CC.1943-5614.0000487.

[12] Hossain KMA, Ametrano D, Lachemi M. Bond Strength of Standard and High-Modulus GFRP Bars in High-Strength Concrete. J Mater Civ Eng 2014;26(3): 449–56. https://doi.org/10.1061/(ASCE)MT.1943-5533.0000758.

[13] Tekle BH, Khennane A, Kayali O. Bond Properties of Sand-Coated GFRP Bars with Fly Ash-Based Geopolymer Concrete. J Compos Constr 2016;20(5):04016025. https://doi.org/10.1061/(ASCE)CC.1943-5614.0000685.

[14] Saleh N, Ashour A, Sheehan T. Bond between glass fibre reinforced polymer bars and high - strength concrete. Structures 2019;22:139–53. https://doi.org/10.1016/j.istruc.2019.08.003.

[15] Taha A, Alnahhal W, Alnuaimi N. Bond durability of basalt FRP bars to fiber reinforced concrete in a saline environment. Compos Struct 2020;243:112277. https://doi.org/10.1016/j.compstruct.2020.112277.

[16] Cosenza E, Manfredi G, Realfonzo R. Behavior and Modeling of Bond of FRP Rebars to Concrete. J Compos Constr 1997;1(2):40–51. https://doi.org/10.1061/(ASCE)1090-0268(1997)1:2(40).

[17] Hattori A, Kawasaki K, Miyagawa T, Fujii M. Bond Behaviors of Carbon Fiber Strand and Aramid Fiber Deformed Bar. Non-metallic Reinf. Concr. Struct.: Japan Concrete Institute; 1997. p. 349–56.

[18] Bakis CE, Uppuluri VS, Nanni A, Boothby TE. Analysis of bonding mechanisms of smooth and lugged frp rods embedded in concrete. Compos Sci Technol 1998;58(8):1307–19. https://doi.org/10.1016/S0266-3538(98)00016-5.

[19] Hollý I, Bilčík J, Keseli O, Gažovičová N. Bond of GFRP reinforcement with concrete. Key Eng Mater 2016;691:356–65. https://doi.org/10.4028/www.scientific.net/KEM.691.356.

[20] Rezansoff T, Akanni A, Sparling B. Tensile Lap Splices Under Static Loading: A Review of the Proposed ACI 318 Code Provisions. ACI Struct J 1993;90:374–84.

[21] McCormac JC, Brown RH. Design of Reinforced Concrete. 10th Edition. 2015.

[22] Mains RM. Measurement of the Distribution of Tensile and Bond Stresses Along Reinforcing Bars. ACI J Proc 1951;48:225–52. https://doi.org/10.14359/11882.

[23] Thompson MA, Jirsa JO, Breen JE, Meinheit DF. Behavior of Multiple Lap Splices in Wide Sections. ACI J Proc 1979;76:227–48. https://doi.org/10.14359/6945.

[24] Hamad BS, Mansour MY. Bond Strength of Noncontact Tension Lap Splices. ACI Struct J 1996;93:316–26. https://doi.org/10.14359/9691.

[25] Harajli MH, Salloukh KA. Effect of Fibers on Development/Splice Strength of Reinforcing Bars in Tension. ACI Mater J 1997;94:317–24. https://doi.org/10.14359/315.

[26] Tighiouart B. Bond of Fibre Reinforced Plastic (FRP) Reinforcing Bars Embedded in Concrete (Ph.D. Thesis). University of Sherbrooke; 1997.

[27] Şener S, Baant ZP, Becq-Giraudon E. SIZE EFFECT ON FAILURE OF BOND SPLICES OF STEEL BARS IN CONCRETE BEAMS. J Struct Eng 1999;125(6):653–60. https://doi.org/10.1061/(ASCE)0733-9445(1999)125:6(653).

[28] Esfahani MR, Rangan BV. Influence of transverse reinforcement on bond strength of tensile splices. Cem Concr Compos 2000;22(3):159–63. https://doi.org/10.1016/S0958-9465(00)00005-6.

[29] Michaud D, Fam A. Development Length of Small-Diameter Basalt FRP Bars in Normal- and High-Strength Concrete. J Compos Constr 2021;25(1):04020086. https://doi.org/10.1061/(ASCE)CC.1943-5614.0001107.

[30] Baena M, Torres L, Turon A, Barris C. Experimental study of bond behaviour between concrete and FRP bars using a pull-out test. Compos Part B Eng 2009;40(8):784–97. https://doi.org/10.1016/j.compositesb:2009.07.003.

[31] Davalos JF, Chen Yi, Ray I. Effect of FRP bar degradation on interface bond with high strength concrete. Cem Concr Compos 2008;30(8):722–30. https://doi.org/10.1016/j.cemconcomp.2008.05.006.

[32] Zemour N, Asadian A, Ahmed EA, Khayat KH, Benmokrane B. Experimental study on the bond behavior of GFRP bars in normal and self-consolidating concrete. Constr Build Mater 2018;189:869–81. https://doi.org/10.1016/j.conbuildmat.2018.09.045.

[33] Japan Society of Civil Engineers. Recommendation for Design and Construction of Concrete Structures Using Continuous Fiber Reinforcing Materials. 1997.

[34] Canadian Standard Association. Design and Construction of Building Components with Fiber-Reinforced Polymers (CSA S806-12). Mississauga, Ontario, Canada: 2012.

[35] ACI (American Concrete Institute). Guide for the design and construction of structural concrete reinforced with FRP bars (ACI 440.1R-15). Farmington Hills, Michigan: 2015.

[36] Taha A, Alnahhal W. Bond durability and service life prediction of BFRP bars to steel FRC under aggressive environmental conditions. Compos Struct 2021;269: 114034. https://doi.org/10.1016/j.compstruct.2021.114034.

[37] El Refai A, Abed F, Altalmas A. Bond Durability of Basalt Fiber-Reinforced Polymer Bars Embedded in Concrete under Direct Pullout Conditions. J Compos Constr 2015;19(5):04014078. https://doi.org/10.1061/(ASCE)CC.1943-5614.0000544.

[38] Hassan M, Benmokrane B, ElSafty A, Fam A. Bond durability of basalt-fiber-reinforced-polymer (BFRP) bars embedded in concrete in aggressive environments. Compos Part B Eng 2016;106:262–72. https://doi.org/10.1016/j.compositesb.2016.09.039.

[39] Xiong Z, Wei W, Liu F, Cui C, Li L, Zou R, et al. Bond behaviour of recycled aggregate concrete with basalt fibre-reinforced polymer bars. Compos Struct 2021; 256:113078. https://doi.org/10.1016/j.compstruct.2020.113078.

[40] ACI (American Concrete Institute). Guide for the Design and Construction of Concrete Reinforced with FRP Bars (440.1R-06). Farmington Hills, Michigan: 2006.

[41] Theriaule M, Benmokrane B. Effects of Frp Reinforcement Ratio and Concrete Strength. J Compos Constr 1998;2:7–16.

[42] Kalpana VG, Subramanian K. Behavior of concrete beams reinforced with GFRP BARS. J Reinf Plast Compos 2011;30(23):1915–22. https://doi.org/10.1177/0731684411431119.

[43] Yost JR, Gross SP. Flexural Design Methodology for Concrete Beams Reinforced with Fiber-Reinforced Polymers. ACI Struct J 2002;99:308–16. https://doi.org/10.14359/11914.

[44] Hadhood A, Mohamed HM, Benmokrane B. Experimental Study of Circular High-Strength Concrete Columns Reinforced with GFRP Bars and Spirals under Concentric and Eccentric Loading. J Compos Constr 2017;21(2):04016078. https://doi.org/10.1061/(ASCE)CC.1943-5614.0000734.

[45] Sohail MG, Kahraman R, Al Nuaimi N, Gencturk B, Alnahhal W. Durability characteristics of high and ultra-high performance concretes. J Build Eng 2021;33: 101669. https://doi.org/10.1016/j.jobe.2020.101669.

[46] Canadian Standard Association. Canadian Highway Bridge Design Code (CSA-S6-14). Ontario, Canada: Mississauga; 2014.

[47] ASTM International. ASTM C39: Standard Test Method for Compressive Strength of Cylindrical Concrete Specimens. West Conshohocken, Pennsylvania 2018. https://doi.org/10.1520/C0039_C0039M-18.

[48] ASTM International. ASTM C78 / C78M-18: Standard Test Method for Flexural Strength of Concrete (Using Simple Beam with Third-Point Loading). West Conshohocken, Pennsylvania: 2018. https://doi.org/10.1520/C0078_C0078M-18.

[49] ASTM International. ASTM D7205 / D7205M-06(2016), Standard Test Method for Tensile Properties of Fiber Reinforced Polymer Matrix Composite Bars. West Conshohocken, Pennsylvania: 2016.

[50] Wei W, Liu F, Xiong Z, Lu Z, Li L. Bond performance between fibre-reinforced polymer bars and concrete under pull-out tests. Constr Build Mater 2019;227: 116803. https://doi.org/10.1016/j.conbuildmat.2019.116803.

[51] Zou R, Liu F, Xiong Z, He S, Li L, Wei W. Experimental study on fatigue bond behaviour between basalt fibre-reinforced polymer bars and recycled aggregate concrete. Constr Build Mater 2021;270:121399. https://doi.org/10.1016/j.conbuildmat.2020.121399.

[52] Z. Xiong, Y.Zeng, L.G. Li, A.K.H. Kwan SHH. Experimental study on the effects of glass fibres and expansive agent on the bond behaviour of glass/basalt FRP bars in seawater sea-sand concrete. Constr Build Mater 2021;274:122100. https://doi.org/https://doi.org/10.1016/j.conbuildmat.2020.122100.

[53] Committee A 408. Bond and Development of Straight Reinforcing Bars in Tension (ACI 408R-03). Detroit, Michigan, US: 2003.

[54] Aly R, Benmokrane B, Ebead U. Tensile Lap Splicing of Fiber-Reinforced Polymer. ACI Struct J 2006;103:226–34.